Immune Netw. 2023 Dec;23(6):e48
https://doi.org/10.4110/in.2023.23.e48
pISSN 1598-2629·eISSN 2092-6685

IMMUNE NETWORK

Original Article

Recombinant Human Bone Morphogenetic Protein-2 Priming of Mesenchymal Stem Cells Ameliorate Acute Lung Injury by Inducing Regulatory T Cells

Jooyeon Lee [1], **Jimin Jang** [1], **Sang-Ryul Cha** [1], **Se Bi Lee** [1], **Seok-Ho Hong** [2], **Han-Sol Bae** [3], **Young Jin Lee** [3], **Se-Ran Yang** [1,*]

[1]Department of Thoracic and Cardiovascular Surgery, School of Medicine, Kangwon National University, Chuncheon 24341, Korea
[2]Department of Internal Medicine, School of Medicine, Kangwon National University, Chuncheon 24341, Korea
[3]Cellular Therapeutics Team, Daewoong Pharmaceutical, Yongin 17028, Korea

Received: Sep 18, 2023
Revised: Dec 11, 2023
Accepted: Dec 11, 2023
Published online: Dec 18, 2023

***Correspondence to**
Se-Ran Yang
Department of Cardiovascular Surgery, School of Medicine, Kangwon National University, 1 Kangwondaehak-gil, Chuncheon 24341, Korea.
Email: seran@kangwon.ac.kr

ORCID iDs
Jooyeon Lee
https://orcid.org/0000-0002-4681-7046
Jimin Jang
https://orcid.org/0000-0002-1796-2164
Sang-Ryul Cha
https://orcid.org/0000-0002-9447-6434
Se Bi Lee
https://orcid.org/0000-0003-4691-8127
Seok-Ho Hong
https://orcid.org/0000-0003-3372-442X
Han-Sol Bae
https://orcid.org/0009-0000-5024-3949
Young Jin Lee
https://orcid.org/0000-0002-2325-5271
Se-Ran Yang
https://orcid.org/0000-0002-2422-213X

ABSTRACT

Mesenchymal stromal/stem cells (MSCs) possess immunoregulatory properties and their regulatory functions represent a potential therapy for acute lung injury (ALI). However, uncertainties remain with respect to defining MSCs-derived immunomodulatory pathways. Therefore, this study aimed to investigate the mechanism underlying the enhanced effect of human recombinant bone morphogenic protein-2 (rhBMP-2) primed ES-MSCs (MSC^{BMP2}) in promoting Tregs in ALI mice. MSC were preconditioned with 100 ng/ml rhBMP-2 for 24 h, and then administrated to mice by intravenous injection after intratracheal injection of 1 mg/kg LPS. Treating MSCs with rhBMP-2 significantly increased cellular proliferation and migration, and cytokines array reveled that cytokines release by MSC^{BMP2} were associated with migration and growth. MSC^{BMP2} ameliorated LPS induced lung injury and reduced myeloperoxidase activity and permeability in mice exposed to LPS. Levels of inducible nitric oxide synthase were decreased while levels of total glutathione and superoxide dismutase activity were further increased via inhibition of phosphorylated STAT1 in ALI mice treated with MSC^{BMP2}. MSC^{BMP2} treatment increased the protein level of IDO1, indicating an increase in Treg cells, and $Foxp3^{+}CD25^{+}$ Treg of $CD4^{+}$ cells were further increased in ALI mice treated with MSC^{BMP2}. In co-culture assays with MSCs and RAW264.7 cells, the protein level of IDO1 was further induced in MSC^{BMP2}. Additionally, cytokine release of IL-10 was enhanced while both IL-6 and TNF-α were further inhibited. In conclusion, these findings suggest that MSC^{BMP2} has therapeutic potential to reduce massive inflammation of respiratory diseases by promoting Treg cells.

Keywords: Mesenchymal stem cells; Recombinant human bone morphogenetic protein-2; Acute lung injury; Indoleamine-pyrrole 2,3,-dioxygenase; Regulatory T-cells

IMMUNE NETWORK

Conflict of Interest
The authors declare no potential conflicts of interest.

Abbreviations
ALI, acute lung injury; ARDS, acute respiratory distress syndrome; BALF, bronchoalveolar lavage fluid; BCA, bicinchoninic acid; BMP2, bone morphogenetic protein 2; CCK-8, cell counting kit-8; CM, conditioned medium; DC, dendritic cell; ES-MSC, human embryonic stem cell-derived mesenchymal stem cell; EV, extracellular vesicle; GSH, glutathione; GSSG, glutathione disulfide; IDO1, indoleamine 2,3-dioxygenase-1; iNOS, inducible nitric oxide synthase; LW/BW, lung weight-to-body weight; MSC, mesenchymal stromal/stem cell; MSCBMP2, recombinant bone morphogenic protein-2 primed human embryonic stem cell-derived mesenchymal stem cells; MPO, myeloperoxidase; NO, nitric oxide; PFA, paraformaldehyde; qPCR, quantitative polymerase chain reaction; rhBMP-2, recombinant human bone morphogenetic protein-2; SOD, superoxide dismutase.

Author Contributions
Conceptualization: Lee J, Yang SR; Data curation: Cha SR; Formal analysis: Lee SB; Investigation: Lee J, Yang SR; Methodology: Lee J, Bae HS, Lee YJ; Validation: Jang J, Hong SH; Writing - original draft: Lee J; Writing - review & editing: Yang SR.

INTRODUCTION

Innate immune response pathway is activated through pathogen-associated molecular patterns receptors, such as TLR4, which recognizes common pathogens and triggers immune responses. A large number of immune cells such as neutrophils are recruited into alveoli, and they produce pro-inflammatory cytokines and chemokines. LPS, a well-known endotoxin, is found in outer membrane of gram-negative bacteria and commonly used to induce acute lung injury (ALI) experimental models *in vivo* and *in vitro*. Previously, *in vitro* studies have shown that LPS triggers activation of inflammatory mediators which result in oxidative stress consistently with pattern of patients with ALI/acute respiratory distress syndrome (ARDS). IFN-γ is a prominent mediator of immune responses to LPS, and it drives activation of JAK-STAT pathway that plays vital roles in initiating innate and adaptive immune response (1). STAT1 is phosphorylated by LPS-related JAK activation, resulting in up-regulation of pro-inflammatory factors, such as TNF-α, IL-6 and IL-1β.

Despite sustained clinical advances of ALI/ARDS, it is still a leading cause of death in critically ill patients, and its mortality rates consistently reported approximately 40 percent (2). Since pneumonia-associated ALI/ARDS with fatal inflammatory cytokine release are one of the major complications of this disease (3), it has been rapidly increased the need for development of preventive and treatment medications in recent years. Although lung protective ventilation, antibiotic and pharmacologic therapies have been performed as supportive care, there are still no specific and effective treatments for cure of ALI/ARDS (4).

Mesenchymal stem cells (MSCs) are considered to have broad application with reparative, immunomodulatory, and antimicrobial properties. The beneficial effects of MSCs-based therapies have been proposed to be mediated predominantly by paracrine activity such as soluble factors (including cytokines, chemokines or growth factors) and extracellular vesicles (EVs) secreted from MSCs (5). A few studies described the response of patients with ARDS to MSCs, however the clinical effects have not shown to provide significant improvement in ARDS (6,7). Moreover, the MSCs derived from adult tissues are hampered by a number of limitations in donor heterogeneity and variable cell characteristics (8,9). Accordingly, it is critical to produce and maintain MSCs derived from standardized sources to investigate the efficacy of safety of MSCs in the clinical application of ALI/ARDS. Recently, human embryonic stem cell-derived mesenchymal stem cells (ES-MSCs) are emerging an unlimited source for MSCs, which overcome the limitations experienced with primary MSCs (10).

Bone morphogenetic protein 2 (BMP2) is a multi-functional growth factor involved in embryonic development and cellular functions, and it belongs to the TGF-β superfamily (11). To date, a few studies have indicated that BMP2 increases MSC growth and EV release (12,13). In LPS exposed rats, BMP2 transduced endothelial progenitor cells effectively attenuated pulmonary edema, and recombinant BMP2 infusion inhibited the remodeling of pulmonary arterioles leading to alleviate the inflammation via down-regulation of p21 and caspase-3 activation (14,15). However, the BMP2-induced effects of MSC infusion in alveolar damage is not fully explained, and it is required further mechanism of rhBMP-2 primed MSCs in the progression of ALI.

Maintenance of alveolar homeostasis after lung injury is imperative to primarily restore lung functions as an innate defense system, and failure to repair can result in the acceleration toward ARDS (16). In this context, Tregs plays a critical role in resolution phase from ALI.

Several studies have shown that Tregs are elevated in patients with ALI, and suggested Tregs as playing critical prosurvival, immune suppressive and anti-inflammatory role in ALI. Tregs activations or expansion can promote indoleamine 2,3-dioxygenase-1 (IDO1) expression in immune cells including dendritic cells (DCs) and macrophages. IDO1 is an enzyme that catalyzes the degradation of tryptophan along the kynurenine pathway, and upregulation of IDO1 in DCs and macrophages is associated with immunomodulatory effect through Tregs expansion and T cell suppression (17,18). In this study, we hypothesized that priming MSC with BMP-2 exerts immune modulation via the activation of Tregs. It suggests a potential mechanism wherein it exhibits superior alleviating effects on ALI compared to naïve MSCs.

MATERIALS AND METHODS

Reagents

Recombinant human BMP2 was provided by Daewoong Pharmaceutical Co., Ltd. (Seoul, Korea). Primary Abs against β-actin (#3700), p-STAT1 (Ser701) (#7649s), p-STAT1 (Tyr727) (#9177s), total STAT1 (#9172s) were purchased from Cell Signaling Technology Inc. (Beverly, MA, USA), and inducible nitric oxide synthase (iNOS, sc-650) and IDO (sc-53978) were purchased from Santa Cruz Biotechnology, Inc. (Santa Cruz, CA, USA). Secondary Abs were purchased from Invitrogen (Carlsbad, CA, USA; mouse: 31430; rabbit: 32460). FACS Abs against HLA-DR (307603). CD4 (100411), CD25 (101907), and FOXP3 (320007) were purchased from BioLegend, Inc. (San Diego, CA, USA), and CD105 (560839), CD45 (560973), CD34 (560940), and CD73 (561014) were purchased from BD Biosciences (San Jose, CA, USA).

Cell culture

Human ES-MSCs were provided by Daewoong Pharmaceutical Co., Ltd. ES-MSCs were cultured in a StemPro® MSC SFM XenoFree (Gibco, Waltham, MA, USA) supplemented with 1% L-glutamine (Gibco) and 1% penicillin/streptomycin on the Corning® CellBIND® surface cell culture plates (Corning Inc., Corning, NY, USA) at 37°C. For priming with rhBMP-2, cells were treated with rhBMP-2 (100 ng/ml) for 24 h. All experiments were performed using ES-MSCs at passage number 12. RAW264.7, murine macrophage cell line, was purchased from Korean Cell Line Bank (KCLB, Seoul, Korea). RAW264.7 cells were grown in RPMI-1640 medium at 37°C. To determine immunomodulation effect by paracrine factors from rhBMP-2-primed ES-MSCs in RAW264.7, cells were seeded in 60 mm culture dish at confluency 70%–80%. RAW264.7 cells were incubated with conditioned medium (CM) from ES-MSCs/rhBMP-2-primed ES-MSCs mixed with RPMI1640 (2:1 ratio). After 2 h, LPS was added for 6 h. Cells were lysed with RIPA buffer for western blotting analysis, and CM was used for ELISA.

Animal study design

Animal studies have been accomplished according to the guidelines of the Kangwon National University and approved and followed the regulations of the Institutional Animal Care and Use Committee (IACUC No. KW-210203-2). All mice were purchased from Doo Yeol Biotech (Seoul, Korea), and housed in a temperature- and humidity-controlled room with a constant photoperiod (12 L:12 D). To establish ARDS/ALI mice model, 8-week-old mice were anesthetized by 10% Zoletil (Virbac Corp., Westlake, TX, USA) 200 μl, after then, 1 mg/kg LPS from *Escherichia coli* O26:B6 (Sigma, St. Louis, MO, USA) or saline (control) were injected intratracheally. After 4 h LPS injection, 1×10^5 ES-MSC (MSC), rhBMP-2-primed ES-MSCs (MSC^{BMP2}) in 100 μl saline were administrated into the tail vein. At 24 h after LPS injection, mice were sacrificed. To harvest the bronchoalveolar lavage fluid (BALF), mice tracheas

were immediately cannulated with 18 G catheter and the lungs were rinsed 2 times with 1 ml saline. Cells were centrifuged at 3,000 rpm for 10 min at 4°C, and supernatants were used immediately or stored at −80°C. For sampling lung tissue, all lobes of mice lung except left lung were snap-frozen with liquid nitrogen (for homogenization), and left lung was stored in 4% paraformaldehyde (PFA) (fixation). To evaluate the survival rate of experimental mice, mice were intratracheally injected with 40 mg/kg LPS. After 4 h LPS injection, 1×10^5 ES-MSCs and rhBMP-2 ES-MSCs were administrated into the mice tail vein, and they were monitored for 4 days.

Cell viability assay

ES-MSCs were seeded at 1×10^5 cells/well in 24-well CellBIND® plate with culture media with/without BMP2 (0, 50, 100 and 200 ng/ml) for 24 h. Furthermore, ES-MSCs were seeded at 5×10^4 cells/well in 24-well CellBIND® plate and treated with BMP2 (0, 50, 100, 200, 400, and 1,000 ng/ml) for 7 days to check cell viability by long-term treatment of BMP2. For MTT assay, 0.1 mg/ml MTT solution (Sigma) was added to each well further incubated for 2 h at 37°C. The supernatant was removed, and then 500 µl of DMSO was added to each well to dissolve the purple formazan crystals. The crystals were measured by platEpoch (BioTek, Winooski, VT, USA) microplate spectrophotometer at 540 nm. For WST-8 assay, we used the cell counting kit-8 (CCK-8) (CK04-11) (Dojindo Molecular Technologies, Inc., Rockville, MD, USA), and performed according to the manufacturer's protocol. Cell viability was calculated as follows: Cell Viability (%) = $(A_{treatment}-A_{blank})/(A_{control}-A_{blank})\times100\%$, A=absorbance, OD value.

Migration assay

Cell migration was determined by transwell assay and wound-healing assay. For the transwell assay, 1×10^5 cells/well were seeded in 300 µl StemPro® MSC SFM XenoFree with/without BMP2 (100 ng/ml) on the insert (upper chamber), and 500 µl StemPro® MSC SFM XenoFree with/without BMP2 (100 ng/ml) was added to the lower chamber. The cells were incubated for 24 h at 37°C. All chambers were fixed methanol and stained by Diff-quick staining. The cells on the upper side of the insert were removed by a cotton swab, and then the lower filters of the inserts were demounted carefully using a forceps and scalpel blades. The filters were put on the slide and mounted with Canada balsam. Under a microscope, the cells were counted per field of representative images (×100). For wound-healing assay, 5×10^5 cells/well were seeded in 6-well plate. At 90% confluency, the cell layer was scraped off using 200 µl tips and then cultured in StemPro® MSC SFM XenoFree medium with/without BMP2 (100 ng/ml) for 24 h. The cells were observed under the microscope and captured images at 0 and 24 h.

Cytokine array

The 1×10^6 cells were seeded in CellBIND® T75 flask. After 24 h, BMP2 (100 ng/ml) was treated into the cells for 24 h. The CM of ES-MSCs and BMP2-primed ES-MSCs were used for cytokine array (Human XL Cytokine Array Kit, ARY022B) (R&D Systems, Minneapolis, MN, USA). The procedure was performed according to the manufacture instructions. At the end of step, the membranes conjugated with the antigens/Abs were visualized on a BioRad ChemiDoc™ imaging system (Bio-Rad, Hercules, CA, USA). Then, all of dot were quantified by Image Lab software (ver. 6.0.1.; Bio-Rad) and generated as a heatmap clustering.

Histological analysis

Harvested lung lobes were washed in ice-cold 1× PBS, and then immediately fixed with 4% PFA overnight at room temperature. The lungs were paraffin-embedded and cut into 4 µm sections. Lung sections were subsequently stained with H&E, then observed under

https://doi.org/10.4110/in.2023.23.e48

a microscope. Lung injury scoring test was performed in a blinded fashion based on 4 histological parameters: infiltration of neutrophils, thickening of alveolar walls, congestion, edema. The histological severity was graded from 0 (normal) to 4 (severe), and the total score was calculated (19).

Myeloperoxidase (MPO) activity

To detect MPO activity, lung tissue homogenized in 0.5 mL of 0.5% hexadecyltrimethyl ammonium bromide in 50 mM potassium phosphate buffer (pH 6.0). The homogenate was centrifuged at 13,000 rpm for 15 min at 4°C. The supernatant or BALF was added with *o*-dianisidine solution (3u,3′-dimethoxybenzidine dihydrochloride in potassium phosphate buffer, pH 6.0) and determined at 450 nm using an Epoch microplate spectrophotometer (BioTek). MPO activity (unit/mL) was calculated in following formula.

$$Unit/mL = \frac{(OD_{Sample} - OD_{Blank}) \times Dilution factor}{Enzyme\ Volume\ (ml)}$$

Total protein in BALF

Total protein concentration in BALF was measured by Pierce™ bicinchonicic acid (BCA) protein assay kit (cat. 23227) (Thermo Fisher Scientific, Waltham, MA, USA). The procedure was performed according to the manufacture instruction. In brief, each 10 μl BALF and BSA (standard) were replicated into 96-well plate. Next, 200 μl working reagent mixture were added in each well for 30 min at room temperature, and they were measured at 540 nm using an Epoch microplate spectrophotometer (BioTek).

BALF cell staining

Isolated BALF was centrifuged at 3,000 rpm for 10 min. Cell pellets were resuspended with 1 ml 1× PBS, then resuspended cells (100 μl) were cyto-centrifuged on poly-L-lysine-coated slides at 3,000 g for 10 min (Sigma). The cells were stained using CAMCO® Stain Pak kit (cat. 702) (Cambridge Diagnostic Products, Fort Lauderdale, FL, USA) according to manufacture's protocol. Slides were observed, and each cell were counted under a microscope.

ELISA

To determine inflammatory cytokines in BALF and cell CM, we used R&D Duoset® ELISA kit (mTNF-α, DY-410; mIL-6, DY-406; mIL-1β, DY-401; mIL-10, DY-417; hIL-10, DY217B-05; hIL-6, DY-206; hTNF-α, DY-210) (R&D System). All Abs were coated in Maxisorp Nunc-immuno modules microplate (Thermo Fisher Scientific) overnight. Each procedure was performed according to manufacture instruction. The sulfuric acid solution (Daejung Chemicals & Metals, Siheung, Korea) was used to stop the colorimetric subtractive process. The absorbance was detected at 450 nm using platEpoch microplate spectrophotometer.

Western blot analysis

Mice lung tissues and RAW264.7 cells were lysed by RIPA buffer; supernatants were harvested to isolate protein. The 25 μg protein was quantified by BCA protein assay, and then, the samples were prepared with 5X SDS sample buffer (BSS-9005) (Tech & Innovation, Chuncheon, Korea). Protein was separated in 10%–15% SDS-acrylamide gel, and transferred onto a nitrocellulose transfer membrane 0.45 mm (Bio-Rad). The membrane was blocked with 5% skim-milk in 1X TBST for 1 h. First Ab was incubated for 4 h at room temperature or overnight at 4°C, and 2nd Ab was incubated for 1 h. First Abs purchased from SantaCruz were diluted 1:1,000; 1st Abs purchased from Cell Signaling were diluted 1:2,000; 1st Ab against

β-actin was diluted 1:10,000. Anti-mouse/rabbit 2nd Abs were diluted 1:2,000. In case of detection against β-actin, 2nd Ab was diluted 1:5,000. After Abs attachment, membrane was washed by 1X TBST, and Ab binding was developed using ECL solution (Bio-Rad). Bands were detected using BioRad ChemiDoc™ imaging system (Bio-Rad).

Real-time PCR

mRNA was isolated from mouse lung and ES-MSCs using Trizol (Invitrogen, Waltham, MA, USA). The 1 μg of RNA was revers-transcribed using Reverse Transcription Premix (ELPIS Biotech, Daejeon, Korea). Real-time PCR was performed using SYBR® green on the StepOnePlus™ Real-Time PCR System (Applied Biosystems, Foster City, CA, USA). The expression level of mRNA was quantified by following $2^{(-\Delta\Delta Ct)}$. All primer pairs used in real-time PCR are listed in **Table 1**.

Molecular detection of the human cells by quantitative PCR (qPCR)

Human specific gene, chromosome 17-a was detected to confirm the human cells into the ES-MSCs-injected mice lung by qPCR. Primers for human chromosome 17 were as follows: F: 5′-GGG ATA ATT TCA GCT GAC TAA ACA G-3′; R: 5′-AAA CGT CCA CTT GCA GTT CTA G-3′; mouse GAPDH: F: 5′-CCT GCG ACT TCA ACA GCA AC-3′; R: 5′-TGG GAT AGG GCC TCT CTT GC-3′.

Superoxide dismutase (SOD) activity assay

To determine SOD, we used SOD assay kit (cat. 19160) (Sigma). Samples were prepared at 10 μg protein from lung tissue lysate. All procedures were performed according to manufacture instruction. Each well was read at 450 nm absorbance using platEpoch microplate reader. The SOD activity (inhibition rate %) was calculated using the equation in the manufacture's protocol.

Total glutathione (GSH) measurement

The assay for quantitative determination of GSH and glutathione disulfide (GSSG) levels was conducted as previously described method by Rahman et al. (20). In brief, the mouse lung tissues were homogenated with RIPA buffer. The supernatant concentration was determined by a BCA Assay Kit. The 10 μg protein was mixed with 0.67 mg/ml 5,5'-dithiobis-(2-nitrobenzoic acid) and 10 U/ml GSH reductase. After 30 s, 0.67 mg/ml β-NADPH was added to the sample. The actual total GSH and GSSG concentrations in the sample were determined by calculated linear regression values from a standard curve 4 times every 30 s at 450 nm absorbance.

Table 1. Sequences of the primers in real-time PCR analysis

Species	Genes	Sequence
Mouse	*Nos2*	F: 5′-GGATCTTCCCAGGCAACCA-3′
		R: 5′-TCCACAACTCGCTCCAAGATT-3′
	Ido1	F: 5′-CGATGTTCGAAAGGTGCTGC-3′
		R: 5′-GCAGGAGAAGCTGCGATTTC-3′
	Gapdh	F: 5′-GGCAAATTCAACGGCACAGT-3′
		R: 5′-CGCTCCTGGAAGATGGTGAT-3′
Human	*MMP9*	F: 5′-CATCGTCATCCAGTTTGGTG-3′
		R: 5′-AGGGACCACAACTCGTCATC-3′
	CXCR4	F: 5′-CCCTCCTGCTGACTATTCCC-3′
		R: 5′-TAAGGCCAACCATGATGTGC-3′
	FBXO5	F: 5′-ACCAAGTTATCCAATCAA-3′
		R: 5′-GAATTACAGCGAATACAG-3′
	GAPDH	F: 5′-CAATGACCCCTTCATTGACC-3′
		R: 5′-GACAAGCTTCCCGTTCTCAG-3′

https://doi.org/10.4110/in.2023.23.e48

FACS

To confirm MSC phenotype markers in ES-MSCs and BMP2-primed ES-MSCs, cells were incubated with/without BMP2 (100 ng/ml) for 24 h in CellBIND® 100 mm cell culture dish. After, cells were trypsinized and washed with FACS buffer twice. Cells were transferred in e-tube at density of 1×10^6 cells/100 μl FACS buffer, and they were stained with CD73, CD105, CD45, CD34 and HLA-DR with the respective isotype control Ab (21). To determine Tregs contribution in ES-MSCs and BMP2-primed ES-MSCs-injected ALI mice, spleen was harvested in mouse. The spleen was transferred in a sterile petri dish containing 1X PBS. Then, the spleen was gently pressed using syringe plunger in the petri dish. The pieces of spleen were collected and transferred on 100 μm strainer attached to a conical tube. The transferred pieces of spleen were gently press using the back of a syringe plunger to macerate the cells through the filter, and the filter was rinsed with 1X PBS twice. All procedures were performed on ice. The cells were centrifuged at 3,000 rpm for 10 min. Then, supernatant was discarded, and cells were resuspended in 1 ml PBS and filtered through 100 μm strainer. The cells were centrifuged at 2,000 rpm for 3 min, and then supernatant was removed. 1×10^6 cells were resuspended in 100 μl FACS buffer with CD4 and CD25 Ab conjugated fluorescence dye or fluorescence dye only (negative). After 30 min at room temperature, cells were centrifuged at 3,000 rpm for 3 min, and then washed with FACS buffer. For FOXP3 staining, True-Nuclear™ Transcription Factor Buffer Set (Cat. 424401) (BioLegend) was used. Next procedures were performed according to the manufacture instructions. All labeled cells were analyzed by Accuri-C6 flow cytometry (BD Biosciences).

Statistical analysis

The results are represented as the mean ± SEM. One-way ANOVA followed by Bonferroni's multiple comparison test was used for comparisons between multiple groups. In comparison between 2 experimental samples, unpaired 2-tailed Student's t-test was used.

RESULTS

rhBMP-2 enhanced proliferation and migration of ES-MSCs

We investigated cell surface markers for the characterization of MSC by flow cytometry analysis (22). The majority of MSCs expressed CD93 and CD105 (>90%), while CD34, CD45 and HLA-DR were virtually undetectable (<0.5%) in both non-treated cells (**Supplementary Fig. 1A**) and rhBMP-2-primed cells (**Supplementary Fig. 1B**). To evaluate the effect of rhBMP-2 on cell viability, we initially performed the MTT and CCK-8 assay. After 24 h exposure, rhBMP-2 significantly increased ES-MSCs viability at concentration of 100 ng/ml and 200 ng/ml (**Fig. 1A and B**). The effect of rhBMP-2 on the vertical and horizontal migration of MSCs were measured by the transwell and scratch assays, respectively. As a result, rhBMP-2 significantly improved cell migration capacity of ES-MSCs in both assays (**Fig. 1C-E**). Moreover, rhBMP-2 increased mRNA levels of MSCs migration-related genes including MMP9, FBXO5 and CXCR4 (**Fig. 1F-H**). We next evaluated that rhBMP-2 enhances secretion of soluble factors produced from MSCs as paracrine effect. We performed cytokine array, which displayed quantification of several cytokines production by visualizing as dots (**Supplementary Fig. 2**). Heat-map data represented that rhBMP-2 priming enhanced overall paracrine activity of ES-MSCs (**Supplementary Fig. 2A**); in particular, IL-11, IL-6, PDGF-AB/BB, HGF, dkk1, and TFF3 were considerable among 105 human cytokines (**Supplementary Fig. 2B**). In cytokine array, upregulated factors were mostly related with migration (13 factors) (23-36) and growth (11 factors) (27,30,31,36-41) in ES-MSCs (**Supplementary Fig. 2C**).

https://doi.org/10.4110/in.2023.23.e48

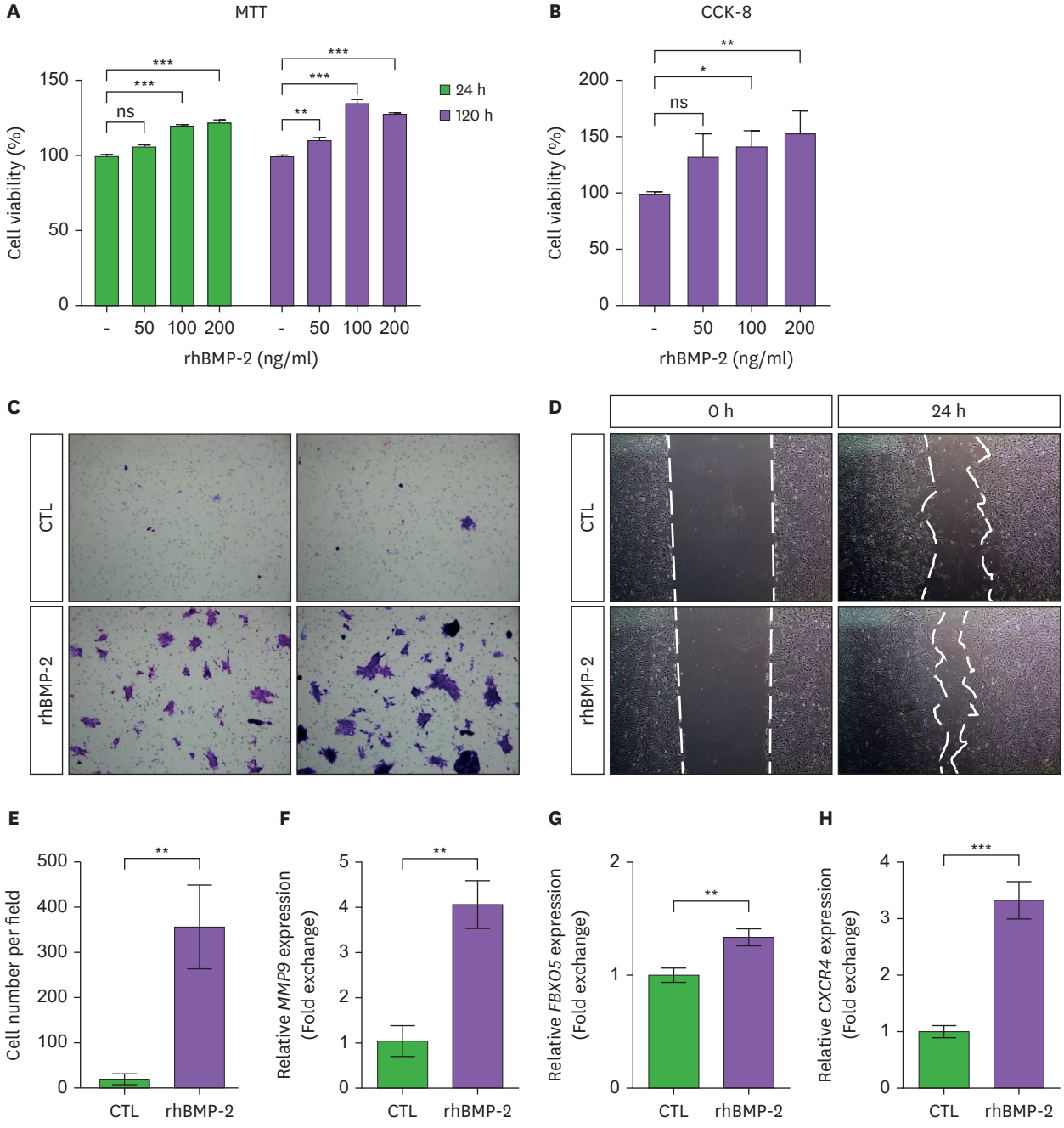

Figure 1. rhBMP-2 enhanced proliferation and migration capacity of ES-MSCs. Cell viability was measured by MTT assay and WST-8 assay. (A) Cells were treated 0, 50, 100 and 200 ng/ml concentration of rhBMP-2 for 24 h and 120 h in MTT assay. (B) In WST-8 assay, cells were treated 0, 50, 100, and 200 ng/ml rhBMP-2 for 24 h. (C) The transwell migration assay and (D) wound healing assay were performed to confirm the improvement of migration ability by rhBMP-2 in ES-MSCs. (E) We counted the cells in the microscope field. (F-H) The mRNA levels of migration-associated genes were detected by real-time PCR. All data are represented as mean ± SD.
ns, not significant.
*p<0.05, **p<0.01, and ***p<0.001 compared with control group.

EVs carry a variety of cargo including DNA, mRNA, micro-RNAs, long non-coding RNAs, protein, lipids, and metabolites. Several studies have shown that EVs derived from MSCs appear therapeutic potentials. Therefore, we isolated EVs from conditioned media to quantify beneficial paracrine ability of ES-MSCs. In NTA analysis, rhBMP-2 further increased EVs

https://doi.org/10.4110/in.2023.23.e48

concentration (particles/ml) suggesting that rhBMP-2 would enhance paracrine potency of ES-MSCs, such as release of EVs (**Supplementary Fig. 2D**). Taken together, our findings suggest that the secretion in MSCs could be enhanced by treatment with rhBMP-2 leading to improve MSC proliferation and migration.

MSC^{BMP2} diminished lung injury in ALI mice

We next determined whether the enhanced migration of MSC^{BMP2} to lung injury improves the therapeutic effect. MSC or MSC^{BMP2} was intravenously injected in mice after injection of LPS. To detect engrafted human cells within mice lung tissue, we performed PCR of human specific a-satellite region of chromosome 17 (850 bp). As a result, both MSC and MSC^{BMP2} were observed in mice lung tissue after 20 h cell injection (**Supplementary Fig. 3**). In a survival analysis, MSC- or MSC^{BMP2}-treated mice were survived until the endpoint of observation (66.7%, 77.8% respectively at 4 days after LPS injection), and only 22.2% mice were survived in the LPS group (**Fig. 2A**). Also, LPS markedly reduced mice body weight. Although MSC and MSC^{BMP2} slightly increased body weight, it was not statistically significant (**Fig. 2B**). Body weight and the lung weight-to-body weight (LW/BW) ratio remained largely unchanged in response to MSC infusion. Conversely, the introduction of MSC^{BMP2} significantly diminished the LW/BW ratio (**Fig. 2C**). In histological analysis, LPS-administrated mice lungs showed infiltration of numerous inflammatory cells, hemorrhage and edema compared with control mice (**Fig. 2D**). Although MSC group also diminished acute injury manifestations, MSC^{BMP2} showed further protective effect than MSC in ALI mice (**Fig. 2D**). We calculated indices of lung injury based on histological observations in **Fig. 2D and E**, MSC^{BMP2} group significantly decreased lung injury score compared with MSC group (**Fig. 2D and E**). Moreover, LPS exposure induced increase of not only MPO enzyme activity that has been considered as an indicator of inflammation and onset of sepsis and mainly expressed in neutrophils, but also total protein in BALF, which reflects vascular permeability (**Fig. 2F and G**) (42). Interestingly, MPO activity in whole lung tissue and BALF, and total protein in BALF were further reduced by MSC^{BMP2} group after LPS injection (**Fig. 2F-H**). Taken together, these data showed that MSC^{BMP2} were detected in the injured lung tissue with enhanced potency and more effectively alleviate ALI.

MSC^{BMP2} transplantation inhibited infiltration of inflammatory cells and pro-inflammatory cytokines

To confirm whether rhBMP-2 could increase anti-inflammatory property of ES-MSC, we harvested BALF and BALF cells from LPS and ES-MSCs treated-mice. Most of BALF cells consisted of macrophages and neutrophils, which were distinguished based on difference of morphology (**Supplementary Fig. 4**). We observed that LPS mediated numerous inflammatory cells, especially neutrophils, and hemorrhage compared with control group (**Fig. 3A**). MSC^{BMP2} transplantation exhibited a remarkable inhibition of inflammatory cells infiltration (**Fig. 3B-D**). Pro-inflammatory cytokines such as TNF-α, IL-1β and IL-6 in BALF were increased by LPS administration. However, MSC^{BMP2} group markedly ameliorated level of all cytokines (**Fig. 3E-G**) while MSC group reduced TNF-α significantly, but not IL-1β and IL-6. These findings indicated that MSC^{BMP2} possesses further enhanced anti-inflammatory properties compared with non-primed ES-MSCs in ALI mice.

MSC^{BMP2} infusion attenuated release of ROS/nitric oxide (NO) and STAT1 activation in ALI mice

ROS and NO are generated by various cells, including leukocytes and parenchymal cells, during acute inflammatory response, and it is believed that oxidative stress following these free radicals has been implicated in the pathogenesis of ARDS or ALI (43,44). Hence,

https://doi.org/10.4110/in.2023.23.e48

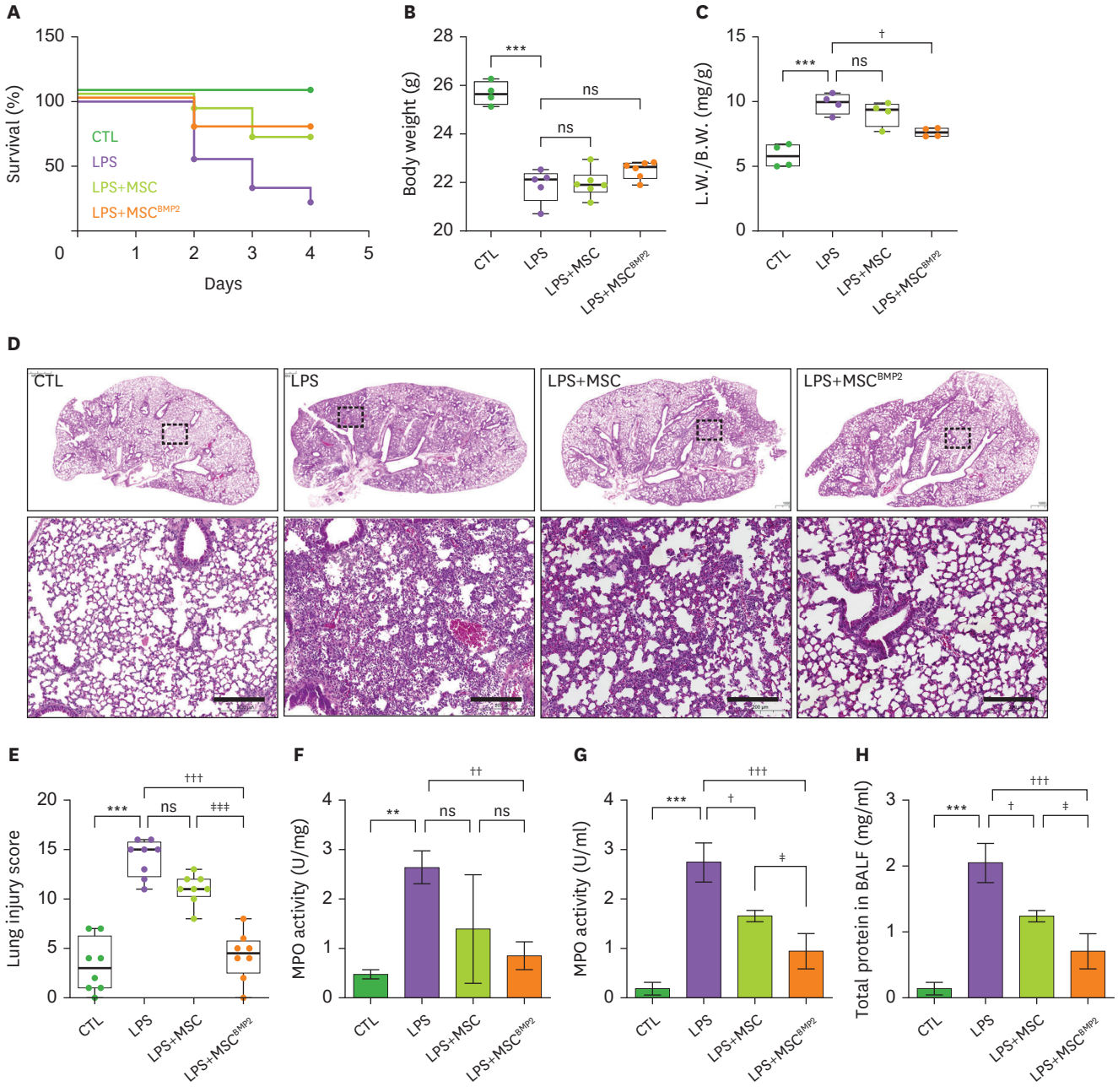

Figure 2. MSC^{BMP2} diminished lung injury in ALI mice. (A) To determine survival rate against ES-MSCs with LPS injection, mice were administrated LPS (40 mg/kg), 4 h after, ES-MSCs and rhBMP-2-primed ES-MSCs were injected to mice (1×10^5) intravenously. For other experiments except survival analysis, mice were injected 1 mg/kg LPS intratracheally, and after 4 h, injected ES-MSCs and rhBMP-2-primed ES-MSCs intravenously (1×10^5). (B) Body weight (g) and (C) the ratio of lung weight to body weight (mg/g) were measured after 24 h LPS injection. (D) Histological analysis was performed by H&E staining under a microscope. Scale bar = 50 μm. (E) The lung injury scores were quantified from histological data. (F) MPO activity was measured in whole lung tissues and (G) BALF (right). (H) Total protein was measured in BALF by BSA assay. All data are represented as mean ± SD.
ns, not significant.
**p<0.01, and ***p<0.001 compared with control group. †p<0.05, ††p<0.01 and †††p<0.001 compared with LPS group. ‡p<0.05, and ‡‡‡p<0.001 compared between LPS+MSC and LPS+ MSC^{BMP2} groups.

we investigated oxidative stress-related signaling in ALI mice. Expression of iNOS, one of enzymes generating NO, was significantly increased by LPS and inhibited by MSC^{BMP2} transplantation in both protein- and mRNA levels. Although MSC group tended to decrease iNOS, these results were not statistically significant (**Fig. 4A-C**). In addition, antioxidant

https://doi.org/10.4110/in.2023.23.e48

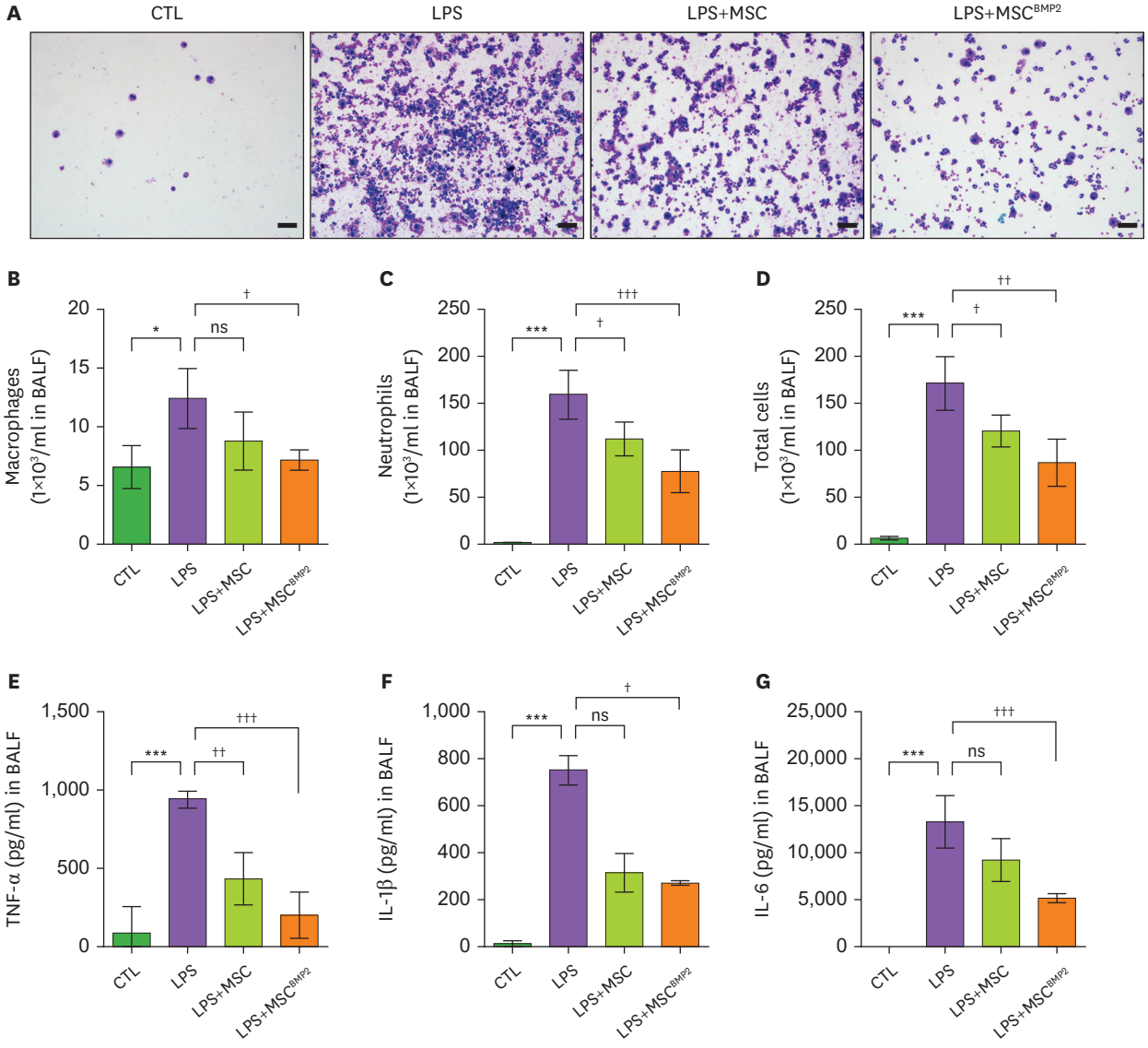

Figure 3. MSC^{BMP2} inhibited infiltration of inflammatory cells and cytokines. Mice were injected 1 mg/kg LPS intratracheally, and after 4 h, injected ES-MSCs and rhBMP-2-primed ES-MSCs intravenously (1×10^5). (A) In the BALF, cells were harvested and stained by Diff-quick staining. Scale bar = 50 μm. (B) Macrophages, (C) neutrophils and (D) total cells were counted under a microscope. Inflammatory cytokines in BALF, including (E) TNF-α, (F) IL-1β, and (G) IL-6 were detected by ELISA. All data are represented as mean ± SD.
ns, not significant.
*p<0.05, and ***p<0.001 compared with control group. †p<0.05, and †††p<0.001 compared with LPS group. ‡p<0.05, and ‡‡‡p<0.001 compared with LPS+MSC group.

enzymes, GSH peroxidase; GSH, and superoxide mutase; SOD, activity levels were recovered by MSC^{BMP2} after LPS injury (**Fig. 4D and E**). We previously elucidated that LPS injury highly mediated recruitment of neutrophils in which IFN-γ signaling pathway is activated leading to up-regulation of STAT1 (45). We next confirmed that LPS increased phosphorylation Tyr701 and Ser727 on STAT1. Furthermore, MSC^{BMP2} markedly decreased STAT1 phosphorylation (**Fig. 4F and G**). These findings suggest that MSC^{BMP2}, compared to MSC, attenuates oxidative damage and inhibits STAT1 signaling activation in ALI mice.

https://doi.org/10.4110/in.2023.23.e48

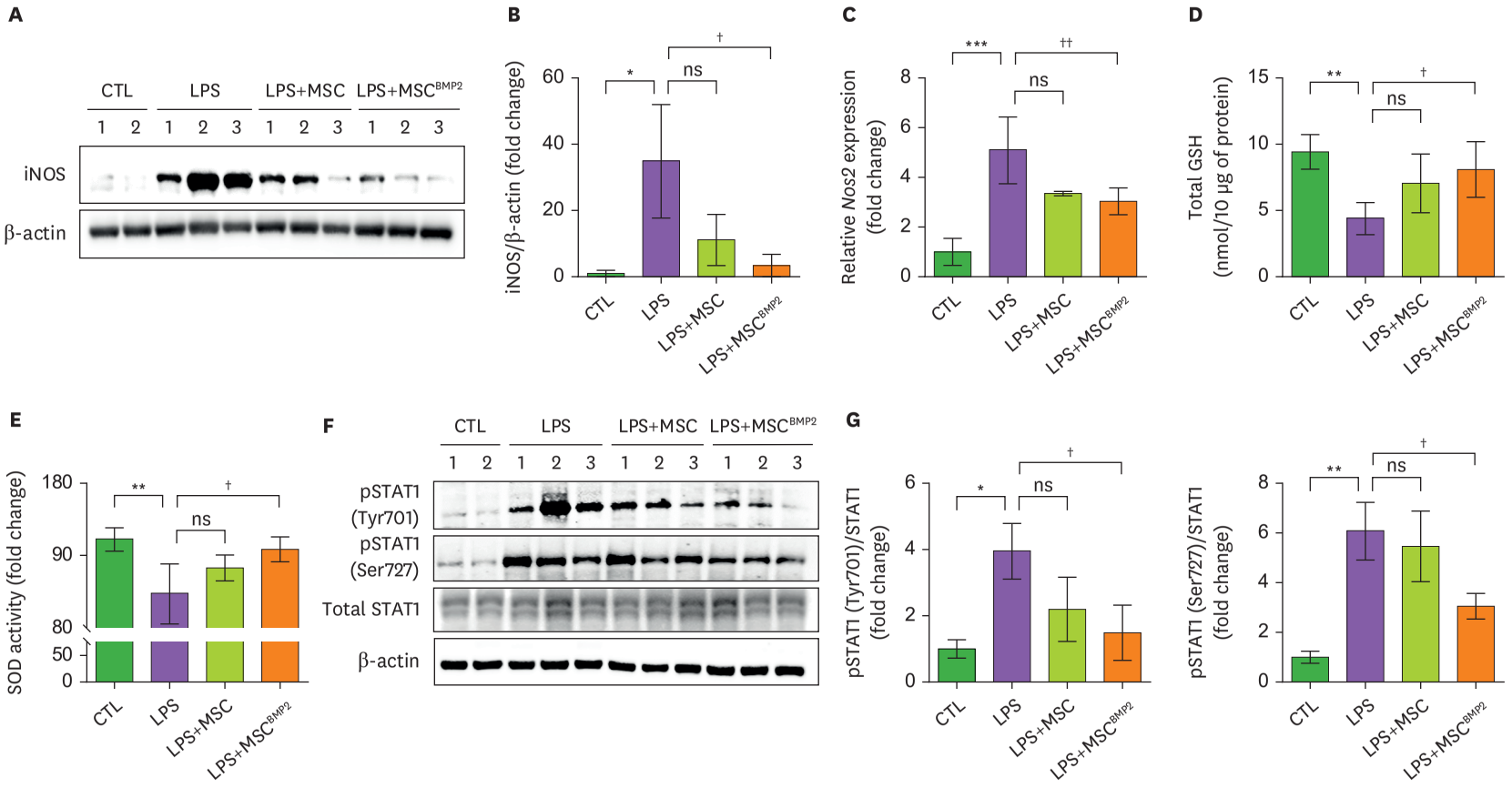

Figure 4. MSC^{BMP2} attenuated ROS/NO and STAT1 activation. Mice were injected LPS 1 mg/kg, after 4 h, MSC and MSC^{BMP2} were injected intravenously (1×10^5). (A) Western blot analysis showed iNOS expression in mouse lung tissue, quantified as (B) densitometric ratio of iNOS against β-actin by ImageJ software. (C) At mRNA level, *Nos2* expression was measured by real-time PCR. To determine anti-oxidative activity, (D) total GSH and (E) SOD activity was analyzed in lung tissue homogenates. (F) Western blot analysis was performed for phosphorylated STAT1 (Ser701 and Tyr727), total STAT1 and β-actin, and quantified as (G) densitometric ratio of phosphorylated STAT1, at Ser701 and tyr707, against β-actin. All data are represented as mean ± SD.
ns, not significant.
*p<0.05, **p<0.01, and ***p<0.001 compared with control group. †p<0.05, and ††p<0.01 compared with LPS group.

MSC^{BMP2} enhanced macrophage-derived IDO1 and Tregs activation

We next examined whether the released cytokines are involved in the immunomodulation mediated by MSC^{BMP2}. In our secretion profile, several notable factors that exhibited enhancement following rhBMP-2 priming (e.g., IFN-γ, CHI3L1, ICAM-1, TARC, TIM-3) are implicated in T cell inhibition and Tregs activation (46-50). Human MSCs enhance the modulation of the inflammatory microenvironment through the catabolism of tryptophan by IDO1 (51). To assess this, we determined the level of IDO1 in mouse lung tissues. When mice were exposed to LPS, mRNA and protein level of IDO1 were increased in the lung tissue. Interestingly, MSC^{BMP2} group, not MSC, further increased IDO1 at both mRNA and protein levels (**Fig. 5A-C**) compared with LPS group. Therefore, we next investigated whether MSC^{BMP2} up-regulates IDO1 mediated Tregs activation in ALI mice. Tregs were observed as a distinct subset of CD4+ T cells by spleen and CD25+ FOXP3+ T cells were gated in CD4+ T cell population using FACS analysis. Tregs were increased in MSC^{BMP2}-treated mice compared with LPS exposed mice and LPS treated with MSC mice (**Supplementary Fig. 5**, **Fig. 5D and E**). Since IDO1 is significantly induced by MSC^{BMP2} *in vivo*, we next sought to validate the expression of IDO1 *in vitro*. To accumulate enough paracrine factors derived from cells, ES-MSCs were primed with rhBMP-2 for 48 h. We subsequently harvested CM and added it into RAW264.7 cells after LPS exposure (**Fig. 5F**). IDO1 level was increased in RAW264.7 cells treated with MSC^{BMP2} CM compared with MSC CM-treated cells (**Fig. 5G and H**). In ELISA, IL-10, was increased in MSC-CM, and MSC^{BMP2}-CM treatment further increased level of IL-10 in LPS-exposed RAW264.7 (**Fig. 5I**). On the other hand, pro-inflammatory cytokines, IL-6 and TNF-α, were significantly decreased by MSC^{BMP2}-CM compared to MSC-CM (**Fig. 5J and K**). In addition, we validated whether rhBMP-2 allows ES-MSCs to produce cytokines. Regarding the concentration of rhBMP-2 (100 ng/ml) for preconditioning, we compared the effect of single rhBMP-2 treatment in ES-MSCs and RAW264.7 cells. Single rhBMP-2 treatment did not change IDO1 expression and cytokine releases of IL-10, IL-6 and TNF-α (**Supplementary Fig. 6**). These findings suggest that MSC^{BMP2} secreted factors particularly enhance IDO1 expression leading to promote Tregs activation with anti-inflammatory effect.

DISCUSSION

In this study, we determined the effect of rhBMP-2 in ES-MSCs and a pivotal role of MSC^{BMP2} to facilitate modulation of T cells for ALI treatment. Despite to therapeutic potential of MSCs, human primary MSCs, in particular those from aged donors, have a limitation of proliferation capacity and donor dependent variations. ES-MSCs have superior to maintain high consistency, addressing the issue of their variations. Moreover, it is beneficial to be processed from bench to bedside according to Good Manufacturing Practices production facilities. Recently, it has shown that priming approaches to improve the efficacy of MSCs with cytokines, growth factors, or hypoxia (52). Here, we sought to apply "priming strategy" in therapeutic approach based on ES-MSCs for ARDS/ALI. Ability to proliferate in stem cells is regarded as a critical factor in terms of successive engraftment and survival, determining treatment efficiency. Accordingly, we observed that rhBMP-2 exhibits significant increase of proliferation rate in short-term condition as well as culture for 5 days. It has shown that rhBMP-2 is associated with osteogenic differentiation capacity of BM-MSCs, and systemic rhBMP-2 treatment increased the number of MSCs while inhibiting MSCs apoptosis in osteopenic mice. Despite rhBMP-2 administration promotes proliferation of MSCs obtained from osteopenic mice, rhBMP-2 induced functional modulation of MSCs remains unknown. Major therapeutic capacity of MSCs is the "homing" toward damaged tissue so that they

https://doi.org/10.4110/in.2023.23.e48

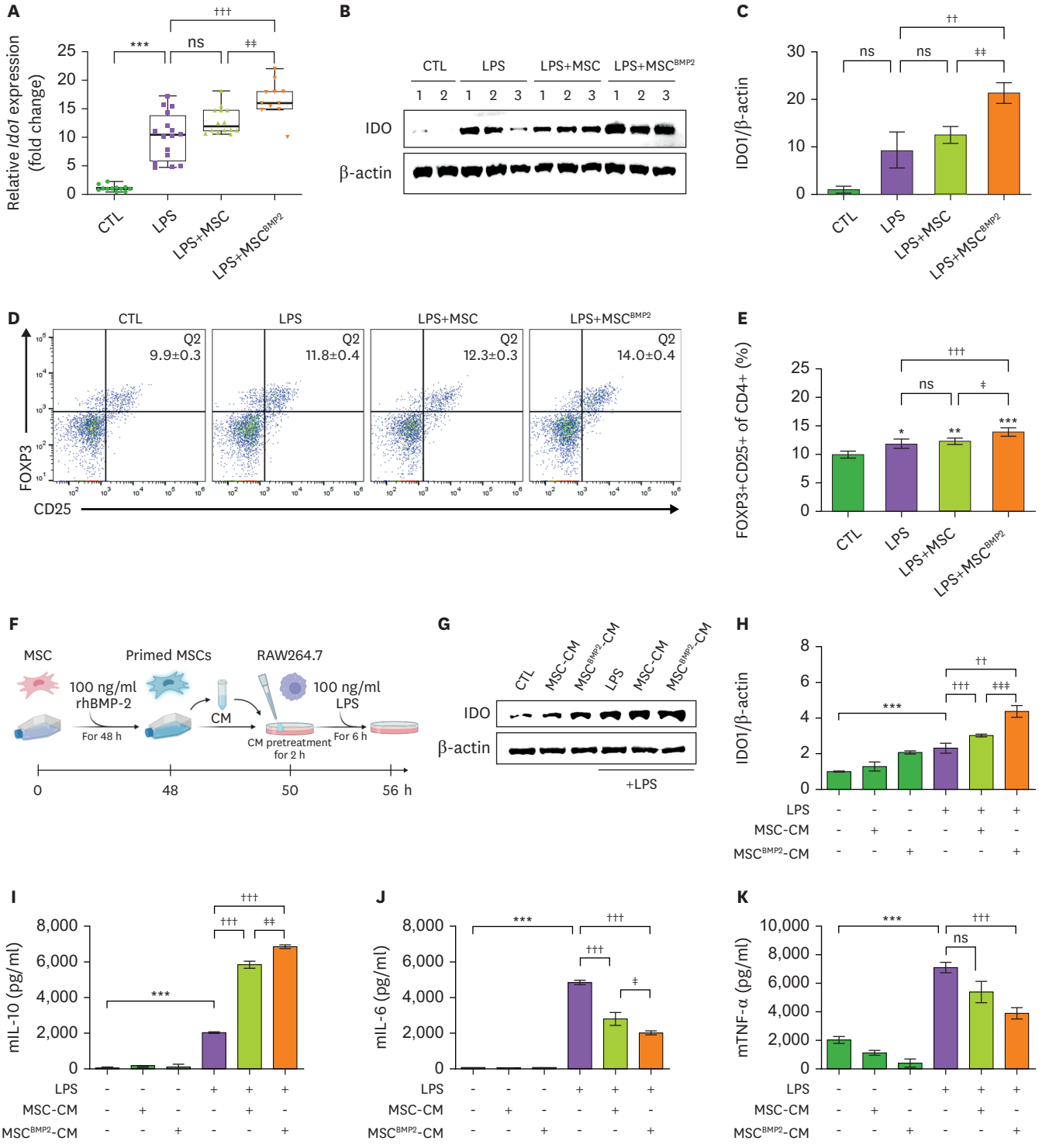

Figure 5. MSC^{BMP2} enhanced macrophage-derived IDO1 and Tregs activation. Mice were injected LPS 1 mg/kg, after 4 h, MSC and MSC^{BMP2} were injected intravenously (1×10^5). (A) In the mouse whole lung tissues, *Ido1* mRNA expression was measured by real-time PCR. (B, C) IDO protein level was measured in western blot analysis. (D) In mouse spleen, FOXP3+CD25+ of CD4+ Treg cells were measured by FACS analysis. (E) The frequency of FOXP3+CD25+ of CD4+ cells (%) was displayed as a graph. All data are represented as mean ± SD. (F-I) CM-derived control or rhBMP-2-treated ES-MSCs was treated into murine macrophage cell line, RAW264.7, for 2 h. The 100 ng/ml LPS was added in culture medium. (G, H) Western blotting analysis for IDO in RAW264.7. (I) Anti-inflammatory cytokine, IL-10, and pro-inflammatory cytokines, (J) IL-6 and (K) TNF-α in CM from RAW264.7 were determined by ELISA. All data are represented as mean ± SD. ns, not significant.

*p<0.05, **p<0.01, and ***p<0.001 compared with control group. ††p<0.01, and †††p<0.001 compared with LPS group. ‡p<0.05, ‡‡p<0.01, and ‡‡‡p<0.01 compared between LPS+MSC and LPS+ MSC^{BMP2} groups.

https://doi.org/10.4110/in.2023.23.e48

produce a large amount of paracrine factors for tissue recovery and regeneration (53). In trans-well- and scratch assay, our results showed that rhBMP-2 promotes cell migration with up-regulation of migration-related genes including MMP9, FBXO5 and CXCR4. In various cell types, MMP9 has been shown to be involved in cell migration (54), and FBXO5 and CXCR4 in MSCs migration. Since the survival and migration of MSCs at the site of the lesion is limited, it is proposed that paracrine factors (i.e., cytokines, chemokines, extravesicles) are critical and considered as primary mechanism of their therapeutic effect. Our data revealed that rhBMP-2 increased cytokine secretion profile which are mostly involved in MSC growth, proliferation and migration. IL-11 and IL-6 (members of IL-6 cytokine family) are well known pro-inflammatory cytokines, whereas both had been identified to be related with MSC proliferation and migration (37,55). Moreover, we observed that EVs released from ES-MSCs were increased by pre-conditioning with rhBMP-2. EV includes a various type of vesicles, such as exosomes and microvesicles, which is recognized as a pivotal mediator of cell-to-cell communication involved in repair processes and disease progression (56). Recent studies suggest that substantial therapeutic mechanism of MSCs is paracrine signaling, dependent on EVs. Although we showed that rhBMP-2 increased paracrine effects including release of EVs and soluble proteins (i.e., cytokines and growth factors), further investigation of specific mechanism through paracrine signaling is needed.

We next determined the effect of rhBMP-2 primed MSCs (MSC^{BMP2}) in ALI mice. MSC^{BMP2} presented to diminish LPS-induced tissue injury and inflammation responses than non-primed ES-MSCs. Previously, Wu et al. (51) described that MSCs could release immunomodulatory factors during an immune response to the inflammatory cytokines produced by T cells and antigen-presenting cells. The MSC-like cells named IMRCs exhibited that T cell-suppressive IDO1 is increased in IMRCs, possessing a hyper immunomodulatory capacity. Indeed, it has been reported that IDO1 is one of paracrine and immunomodulatory factors that play a role in MSC-mediated suppression of T-cell proliferation via Treg activation (57). Therefore, we investigated whether rhBMP-2 increases immunosuppressive capacity of ES-MSCs by analyzing IDO1 expression in the cells; however, level of IDO1 did not changed in ES-MSCs after pre-conditioning of rhBMP-2. On the other hand, we found that LPS slightly increased ido1 in mice lung, and MSC^{BMP2} administration induced further increase of mRNA and protein levels of ido1. Several studies have reported that inflammatory mediators, such as IFN-γ, stimulate expression of IDO1 (58). Inflammatory cytokines stimulate IDO1 to activate host's innate defense mechanism by depleting tryptophan, which acts in apoptosis of CD4+T cells sensitively (59). Furthermore, inflammatory response triggers an anti-inflammatory response mediated via the activation of IDO1-KYN-AhR signaling, resulting in induction of immunosuppressive factors, such as IL-10, TGF-β and FOXP3 (60). Tregs have been highlighted in ALI due to their roles in immune homeostasis, anti-inflammation and repair of damaged tissues. According to Mock and colleagues suggested that the number of Tregs increases after lung injury leading to inflammatory resolution and improvement of alveolar epithelial cells proliferation (61). Consistent with previous studies, our data showed that LPS induced slight increase of Tregs. Moreover, MSC^{BMP2} further increased Tregs population than single LPS-administrated mice, suggesting that MSC^{BMP2} possess enhanced immunosuppressive capacity through IDO1 and Tregs activation. In addition, these findings suggest that MSC^{BMP2} increases IDO1 in certain cell types in the lung, not in itself, and which helps activation of Tregs. Although IDO1 is widely expressed in various cell types, its expression in macrophages and DCs has been reported to be especially relevant with modulation of T cell behavior (62). Under inflammatory conditions, IDO1 can be activated in macrophages to control immune system (63). In this study, we determined mouse macrophage cell line, RAW264.7, to investigate expression of

https://doi.org/10.4110/in.2023.23.e48

IDO1 in macrophages. Interestingly, IDO1 was further increased in RAW264.7 treated with MSC^{BMP2}-CM compared with LPS- and LPS+MSC-CM treated cells. Furthermore, we observed that high level of anti-inflammatory cytokine, IL-10 was produced in MSC^{BMP2}-CM-treated RAW264.7 cells. These observations indicate that not rhBMP-2 increase IL-10 in ES-MSCs but MSC^{BMP2} allow macrophages to produce secretion of IL-10. Taken together, we demonstrated that MSC^{BMP2} are available to modulate host immune response and inhibit inflammation by regulating macrophages or Tregs. Accordingly, our findings are needed further to seek specific factor regulate immunomodulatory mechanism associated with IDO1. In this study, our data suggest that paracrine factors increased by rhBMP-2 priming might be facilitated for ALI treatment. In this study, we demonstrated that BMP2 priming not only enhances the immunomodulatory function inherent in naïve MSCs but also leads to an overall improvement in cellular capabilities. This technique has the potential to address the limitations of previous MSC therapy, such as low yield and diminished therapeutic efficacy. It could be a cost-effective and safe approach that may overcome the limitations, offering a promising solution to enhance the effectiveness of MSC-based therapies in the future.

Taken together, rhBMP-2 promoted proliferation, migration, and paracrine capacity of ES-MSCs. MSC^{BMP2} inhibited tissue impairment, inflammation, dysregulated oxidative homeostasis, STAT1 activation after ALI *in vivo*. In addition, MSC^{BMP2} allowed mice macrophage to release anti-inflammatory cytokine, IL-10; and highly expressed IDO1 resulting in Tregs activation. Taken together, MSC^{BMP2} and its associated cellular mechanism could contribute to understand immunomodulation and paracrine effect of MSC treatment in pre-clinical approaches.

ACKNOWLEDGEMENTS

This study was supported by the National Research Foundation of Korea (NRF) funded by the Ministry of Education, Science and Technology (NRF-2017M3A9B4051542, 2020R1A2C2010712, 2020R1A5A8019180 and 2022M3A9E4016936, RS-2023-00225239), Particulate Matter Management Specialized Graduate Program through the Korea Environmental Industry & Technology Institute(KEITI) funded by the Ministry of Environment(MOE) and Daewoong Pharmaceutical (120210855).

SUPPLEMENTARY MATERIALS

Supplementary Figure 1

Surface markers of ES-MSCs. Representative histogram of flow cytometric analysis of general MSC markers (positive for CD105 and CD73, and negative for CD34, CD45 and HLA-DR) in (A) MSC and (B) MSC^{BMP2} (gray = isotype control, purple or red = specific cell surface markers). Each percentage of positive population was indicated in the plots.

Click here to view

Supplementary Figure 2

rhBMP-2 allowed ES-MSCs to promote release of paracrine factors. (A) Multiple cytokines were assessed by Proteom Profiler Human XL Cytokine Array Kit (R&D Systems), and heat map showed the expression profiles of soluble proteins in the cell culture supernatants from MSC and MSC^{BMP2} for 24 h. (B) Compared the cultured medium from MSC (CTL)

and MSC^{BMP2}, top 20 ranked up-regulated genes were shown by graph of fold-change in expression, and (C) the top 30 ranked up-regulated genes were categorized 13 categories based on other references. (D) NTA analysis was performed to characterize EVs derived MSC and MSC^{BMP2}. Data are represented as mean ± SD.

Click here to view

Supplementary Figure 3

Detection of human ES-MSCs in mice lungs. Mice were injected LPS with MSC and MSC^{BMP2} after 4 h LPS administration. The injected human cells were detected with human chromosome 17a (850 bp) by quantitative RT-PCR, indicating cell engraftment into mice lung in both LPS+MSC and LPS+MSC^{BMP2} groups. Data are represented as mean ± SD.

Click here to view

Supplementary Figure 4

Histologic image of cells in BALF. Cells were stained by Diff-quick staining, and each cell is distinguished based on morphology. Scale bar = 20 μm.

Click here to view

Supplementary Figure 5

Gating strategy for Tregs isolated from spleens. Tregs are identified as a distinct subset of CD4+ T cells expressing high levels of the CD25 and express FOXP3. Single cells isolated from spleen were stained APC-conjugated CD4, PE-conjugated FOXP3 and FITC-conjugated CD25, and analyzed by FACS. CD4+ cell population was distinguishable from negative control due to APC-expressing (red line), and then CD25+ FOXP3+ cells were gated in CD4+ cell population (upper right quadrant, Q2) (n=3).

Click here to view

Supplementary Figure 6

IDO1 and cytokines alteration against rhBMP-2 in RAW264.7 and ES-MSCs. To confirm whether IDO1 expression and cytokine production were affected by rhBMP-2 in CM, we treated only rhBMP-2 containing medium (not conditioned). (A) IDO protein level was measured in western blot analysis. (B) Densitometric ratio of IDO1 against β-actin by ImageJ software (fold change). (C) In RAW264.7-CM, mIL-10 (pg/ml), (D) mIL-6 (pg/ml) and (E) mTNF-α (pg/ml) were detected by ELISA. To detect human cytokines in MSC-CM, we performed ELISA assay. (F) hIL-10 (pg/ml), (G) hIL-6 (pg/ml), and (H) hTNF-α (pg/ml) were detected in MSC-CM after 24 h rhBMP-2 priming. Data are represented as mean (n=3).

Click here to view

REFERENCES

1. Villarino AV, Kanno Y, Ferdinand JR, O'Shea JJ. Mechanisms of Jak/STAT signaling in immunity and disease. *J Immunol* 2015;194:21-27.
PUBMED | CROSSREF

2. Williams GW, Berg NK, Reskallah A, Yuan X, Eltzschig HK. Acute respiratory distress syndrome. *Anesthesiology* 2021;134:270-282.
PUBMED | CROSSREF
3. Ye Q, Wang B, Mao J. The pathogenesis and treatment of the 'Cytokine Storm' in COVID-19. *J Infect* 2020;80:607-613.
PUBMED | CROSSREF
4. Sauer A, Peukert K, Putensen C, Bode C. Antibiotics as immunomodulators: a potential pharmacologic approach for ARDS treatment. *Eur Respir Rev* 2021;30:210093.
PUBMED | CROSSREF
5. Pierce LM, Kurata WE. Priming with toll-like receptor 3 agonist poly(I:C) enhances content of innate immune defense proteins but not microRNAs in human mesenchymal stem cell-derived extracellular vesicles. *Front Cell Dev Biol* 2021;9:676356.
PUBMED | CROSSREF
6. Wilson JG, Liu KD, Zhuo H, Caballero L, McMillan M, Fang X, Cosgrove K, Vojnik R, Calfee CS, Lee JW, et al. Mesenchymal stem (stromal) cells for treatment of ARDS: a phase 1 clinical trial. *Lancet Respir Med* 2015;3:24-32.
PUBMED | CROSSREF
7. Matthay MA, Calfee CS, Zhuo H, Thompson BT, Wilson JG, Levitt JE, Rogers AJ, Gotts JE, Wiener-Kronish JP, Bajwa EK, et al. Treatment with allogeneic mesenchymal stromal cells for moderate to severe acute respiratory distress syndrome (START study): a randomised phase 2a safety trial. *Lancet Respir Med* 2019;7:154-162.
PUBMED | CROSSREF
8. Fukumitsu M, Suzuki K. Mesenchymal stem/stromal cell therapy for pulmonary arterial hypertension: comprehensive review of preclinical studies. *J Cardiol* 2019;74:304-312.
PUBMED | CROSSREF
9. Han J, Li Y, Li Y. Strategies to enhance mesenchymal stem cell-based therapies for acute respiratory distress syndrome. *Stem Cells Int* 2019;2019:5432134.
PUBMED | CROSSREF
10. Li O, Tormin A, Sundberg B, Hyllner J, Le Blanc K, Scheding S. Human embryonic stem cell-derived mesenchymal stroma cells (hES-MSCs) engraft *in vivo* and support hematopoiesis without suppressing immune function: implications for off-the shelf ES-MSC therapies. *PLoS One* 2013;8:e55319.
PUBMED | CROSSREF
11. Chen D, Zhao M, Mundy GR. Bone morphogenetic proteins. *Growth Factors* 2004;22:233-241.
PUBMED | CROSSREF
12. Huang CC, Kang M, Lu Y, Shirazi S, Diaz JI, Cooper LF, Gajendrareddy P, Ravindran S. Functionally engineered extracellular vesicles improve bone regeneration. *Acta Biomater* 2020;109:182-194.
PUBMED | CROSSREF
13. Cai H, Zou J, Wang W, Yang A. BMP2 induces hMSC osteogenesis and matrix remodeling. *Mol Med Rep* 2021;23:125.
PUBMED | CROSSREF
14. Yin X, Liang Z, Yun Y, Pei L. Intravenous transplantation of BMP2-transduced endothelial progenitor cells attenuates lipopolysaccharide-induced acute lung injury in rats. *Cell Physiol Biochem* 2015;35:2149-2158.
PUBMED | CROSSREF
15. Wang K, Gong J, Pei L, Shan S, Tan W. The effect of rhBMP-2 on pulmonary arterioles remodeling in endotoxin-induced acute lung injury in rats. *Clin Exp Med* 2013;13:187-192.
PUBMED | CROSSREF
16. Cipolla EM, Alcorn JF. Repair of the lung by regulatory T cells. *Am J Respir Cell Mol Biol* 2020;63:405-407.
PUBMED | CROSSREF
17. Forteza MJ, Polyzos KA, Baumgartner R, Suur BE, Mussbacher M, Johansson DK, Hermansson A, Hansson GK, Ketelhuth DF. Activation of the regulatory t-cell/indoleamine 2,3-dioxygenase axis reduces vascular inflammation and atherosclerosis in hyperlipidemic mice. *Front Immunol* 2018;9:950.
PUBMED | CROSSREF
18. Hwang SL, Chung NP, Chan JK, Lin CL. Indoleamine 2, 3-dioxygenase (IDO) is essential for dendritic cell activation and chemotactic responsiveness to chemokines. *Cell Res* 2005;15:167-175.
PUBMED | CROSSREF
19. Park JR, Lee H, Kim SI, Yang SR. The tri-peptide GHK-Cu complex ameliorates lipopolysaccharide-induced acute lung injury in mice. *Oncotarget* 2016;7:58405-58417.
PUBMED | CROSSREF
20. Rahman I, Kode A, Biswas SK. Assay for quantitative determination of glutathione and glutathione disulfide levels using enzymatic recycling method. *Nat Protoc* 2006;1:3159-3165.
PUBMED | CROSSREF

21. Park JR, Kim E, Yang J, Lee H, Hong SH, Woo HM, Park SM, Na S, Yang SR. Isolation of human dermis derived mesenchymal stem cells using explants culture method: expansion and phenotypical characterization. *Cell Tissue Bank* 2015;16:209-218.
PUBMED | CROSSREF

22. Baghaei K, Hashemi SM, Tokhanbigli S, Asadi Rad A, Assadzadeh-Aghdaei H, Sharifian A, Zali MR. Isolation, differentiation, and characterization of mesenchymal stem cells from human bone marrow. *Gastroenterol Hepatol Bed Bench* 2017;10:208-213.
PUBMED

23. Gabrielyan A, Quade M, Gelinsky M, Rösen-Wolff A. IL-11 and soluble VCAM-1 are important components of hypoxia conditioned media and crucial for mesenchymal stromal cells attraction. *Stem Cell Res* 2020;45:101814.
PUBMED | CROSSREF

24. Zepp JA, Zacharias WJ, Frank DB, Cavanaugh CA, Zhou S, Morley MP, Morrisey EE. Distinct mesenchymal lineages and niches promote epithelial self-renewal and myofibrogenesis in the lung. *Cell* 2017;170:1134-1148.e10.
PUBMED | CROSSREF

25. Phipps MC, Xu Y, Bellis SL. Delivery of platelet-derived growth factor as a chemotactic factor for mesenchymal stem cells by bone-mimetic electrospun scaffolds. *PLoS One* 2012;7:e40831.
PUBMED | CROSSREF

26. Chabot V, Dromard C, Rico A, Langonné A, Gaillard J, Guilloton F, Casteilla L, Sensebé L. Urokinase-type plasminogen activator receptor interaction with β1 integrin is required for platelet-derived growth factor-AB-induced human mesenchymal stem/stromal cell migration. *Stem Cell Res Ther* 2015;6:188.
PUBMED | CROSSREF

27. Forte G, Minieri M, Cossa P, Antenucci D, Sala M, Gnocchi V, Fiaccavento R, Carotenuto F, De Vito P, Baldini PM, et al. Hepatocyte growth factor effects on mesenchymal stem cells: proliferation, migration, and differentiation. *Stem Cells* 2006;24:23-33.
PUBMED | CROSSREF

28. He S, Shen L, Wu Y, Li L, Chen W, Hou C, Yang M, Zeng W, Zhu C. Effect of brain-derived neurotrophic factor on mesenchymal stem cell-seeded electrospinning biomaterial for treating ischemic diabetic ulcers via milieu-dependent differentiation mechanism. *Tissue Eng Part A* 2015;21:928-938.
PUBMED | CROSSREF

29. Li A, Xia X, Yeh J, Kua H, Liu H, Mishina Y, Hao A, Li B. PDGF-AA promotes osteogenic differentiation and migration of mesenchymal stem cell by down-regulating PDGFRα and derepressing BMP-Smad1/5/8 signaling. *PLoS One* 2014;9:e113785.
PUBMED | CROSSREF

30. Belotti D, Capelli C, Resovi A, Introna M, Taraboletti G. Thrombospondin-1 promotes mesenchymal stromal cell functions via TGFβ and in cooperation with PDGF. *Matrix Biol* 2016;55:106-116.
PUBMED | CROSSREF

31. Kawata K, Koga H, Tsuji K, Miyatake K, Nakagawa Y, Yokota T, Sekiya I, Katagiri H. Extracellular vesicles derived from mesenchymal stromal cells mediate endogenous cell growth and migration via the CXCL5 and CXCL6/CXCR2 axes and repair menisci. *Stem Cell Res Ther* 2021;12:414.
PUBMED | CROSSREF

32. Noronha NC, Mizukami A, Caliári-Oliveira C, Cominal JG, Rocha JL, Covas DT, Swiech K, Malmegrim KC. Priming approaches to improve the efficacy of mesenchymal stromal cell-based therapies. *Stem Cell Res Ther* 2019;10:131.
PUBMED | CROSSREF

33. Lourenco S, Teixeira VH, Kalber T, Jose RJ, Floto RA, Janes SM. Macrophage migration inhibitory factor-CXCR4 is the dominant chemotactic axis in human mesenchymal stem cell recruitment to tumors. *J Immunol* 2015;194:3463-3474.
PUBMED | CROSSREF

34. Cao G, O'Brien CD, Zhou Z, Sanders SM, Greenbaum JN, Makrigiannakis A, DeLisser HM. Involvement of human PECAM-1 in angiogenesis and *in vitro* endothelial cell migration. *Am J Physiol Cell Physiol* 2002;282:C1181-C1190.
PUBMED | CROSSREF

35. Krüger K, Schmid S, Paulsen F, Ignatius A, Klinger P, Hotfiel T, Swoboda B, Gelse K. Trefoil factor 3 (TFF3) is involved in cell migration for skeletal repair. *Int J Mol Sci* 2019;20:4277.
PUBMED | CROSSREF

36. Sivanathan KN, Gronthos S, Rojas-Canales D, Thierry B, Coates PT. Interferon-gamma modification of mesenchymal stem cells: implications of autologous and allogeneic mesenchymal stem cell therapy in allotransplantation. *Stem Cell Rev Rep* 2014;10:351-375.
PUBMED | CROSSREF

37. Yang W, Zhang S, Ou T, Jiang H, Jia D, Qi Z, Zou Y, Qian J, Sun A, Ge J. Interleukin-11 regulates the fate of adipose-derived mesenchymal stem cells via STAT3 signalling pathways. *Cell Prolif* 2020;53:e12771.
PUBMED | CROSSREF

38. Zhang JM, Feng FE, Wang QM, Zhu XL, Fu HX, Xu LP, Liu KY, Huang XJ, Zhang XH. Platelet-derived growth factor-BB protects mesenchymal stem cells (MSCs) derived from immune thrombocytopenia patients against apoptosis and senescence and maintains MSC-mediated immunosuppression. *Stem Cells Transl Med* 2016;5:1631-1643.
PUBMED | CROSSREF

39. Dorronsoro A, Lang V, Ferrin I, Fernández-Rueda J, Zabaleta L, Pérez-Ruiz E, Sepúlveda P, Trigueros C. Intracellular role of IL-6 in mesenchymal stromal cell immunosuppression and proliferation. *Sci Rep* 2020;10:21853.
PUBMED | CROSSREF

40. Xia W, Xie C, Jiang M, Hou M. Improved survival of mesenchymal stem cells by macrophage migration inhibitory factor. *Mol Cell Biochem* 2015;404:11-24.
PUBMED | CROSSREF

41. Liu XH, Bai CG, Xu ZY, Huang SD, Yuan Y, Gong DJ, Zhang JR. Therapeutic potential of angiogenin modified mesenchymal stem cells: angiogenin improves mesenchymal stem cells survival under hypoxia and enhances vasculogenesis in myocardial infarction. *Microvasc Res* 2008;76:23-30.
PUBMED | CROSSREF

42. Tomonaga T, Izumi H, Yoshiura Y, Nishida C, Yatera K, Morimoto Y. Examination of surfactant protein D as a biomarker for evaluating pulmonary toxicity of nanomaterials in rat. *Int J Mol Sci* 2021;22:4635.
PUBMED | CROSSREF

43. Chow CW, Herrera Abreu MT, Suzuki T, Downey GP. Oxidative stress and acute lung injury. *Am J Respir Cell Mol Biol* 2003;29:427-431.
PUBMED | CROSSREF

44. Kellner M, Noonepalle S, Lu Q, Srivastava A, Zemskov E, Black SM. Ros signaling in the pathogenesis of acute lung injury (ALI) and acute respiratory distress syndrome (ARDS). *Adv Exp Med Biol* 2017;967:105-137.
PUBMED | CROSSREF

45. Lee H, Lee J, Park Y, Kim JH, Eickelberg O, Yang SR. WKYMVm ameliorates acute lung injury via neutrophil antimicrobial peptide derived STAT1/IRF1 pathway. *Biochem Biophys Res Commun* 2020;533:313-318.
PUBMED | CROSSREF

46. Liang C, Jiang E, Yao J, Wang M, Chen S, Zhou Z, Zhai W, Ma Q, Feng S, Han M. Interferon-γ mediates the immunosuppression of bone marrow mesenchymal stem cells on T-lymphocytes *in vitro*. *Hematology* 2018;23:44-49.
PUBMED | CROSSREF

47. Liu Q, Chen X, Liu C, Pan L, Kang X, Li Y, Du C, Dong S, Xiang AP, Xu Y, et al. Mesenchymal stem cells alleviate experimental immune-mediated liver injury via chitinase 3-like protein 1-mediated T cell suppression. *Cell Death Dis* 2021;12:240.
PUBMED | CROSSREF

48. Li X, Wang Q, Ding L, Wang YX, Zhao ZD, Mao N, Wu CT, Wang H, Zhu H, Ning SB. Intercellular adhesion molecule-1 enhances the therapeutic effects of MSCs in a dextran sulfate sodium-induced colitis models by promoting MSCs homing to murine colons and spleens. *Stem Cell Res Ther* 2019;10:267.
PUBMED | CROSSREF

49. Riezu-Boj JI, Larrea E, Aldabe R, Guembe L, Casares N, Galeano E, Echeverria I, Sarobe P, Herrero I, Sangro B, et al. Hepatitis C virus induces the expression of CCL17 and CCL22 chemokines that attract regulatory T cells to the site of infection. *J Hepatol* 2011;54:422-431.
PUBMED | CROSSREF

50. Kim SN, Lee HJ, Jeon MS, Yi T, Song SU. Galectin-9 is involved in immunosuppression mediated by human bone marrow-derived clonal mesenchymal stem cells. *Immune Netw* 2015;15:241-251.
PUBMED | CROSSREF

51. Wu J, Song D, Li Z, Guo B, Xiao Y, Liu W, Liang L, Feng C, Gao T, Chen Y, et al. Immunity-and-matrix-regulatory cells derived from human embryonic stem cells safely and effectively treat mouse lung injury and fibrosis. *Cell Res* 2020;30:794-809.
PUBMED | CROSSREF

52. Kim HN, Shin JY, Kim DY, Lee JE, Lee PH. Priming mesenchymal stem cells with uric acid enhances neuroprotective properties in parkinsonian models. *J Tissue Eng* 2021;12:20417314211004816.
PUBMED | CROSSREF

53. Ullah M, Liu DD, Thakor AS. Mesenchymal stromal cell homing: mechanisms and strategies for improvement. *iScience* 2019;15:421-438.
PUBMED | CROSSREF

54. Legrand C, Gilles C, Zahm JM, Polette M, Buisson AC, Kaplan H, Birembaut P, Tournier JM. Airway epithelial cell migration dynamics. MMP-9 role in cell-extracellular matrix remodeling. *J Cell Biol* 1999;146:517-529.
PUBMED | CROSSREF

55. Pricola KL, Kuhn NZ, Haleem-Smith H, Song Y, Tuan RS. Interleukin-6 maintains bone marrow-derived mesenchymal stem cell stemness by an ERK1/2-dependent mechanism. *J Cell Biochem* 2009;108:577-588.
PUBMED | CROSSREF

56. Park KS, Bandeira E, Shelke GV, Lässer C, Lötvall J. Enhancement of therapeutic potential of mesenchymal stem cell-derived extracellular vesicles. *Stem Cell Res Ther* 2019;10:288.
PUBMED | CROSSREF

57. Zimmermann JA, Hettiaratchi MH, McDevitt TC. Enhanced immunosuppression of t cells by sustained presentation of bioactive interferon-gamma within three-dimensional mesenchymal stem cell constructs. *Stem Cells Transl Med* 2017;6:223-237.
PUBMED | CROSSREF

58. Taylor MW, Feng GS. Relationship between interferon-gamma, indoleamine 2,3-dioxygenase, and tryptophan catabolism. *FASEB J* 1991;5:2516-2522.
PUBMED | CROSSREF

59. Lepiller Q, Soulier E, Li Q, Lambotin M, Barths J, Fuchs D, Stoll-Keller F, Liang TJ, Barth H. Antiviral and immunoregulatory effects of indoleamine-2,3-dioxygenase in hepatitis C virus infection. *J Innate Immun* 2015;7:530-544.
PUBMED | CROSSREF

60. Salminen A. Role of indoleamine 2,3-dioxygenase 1 (IDO1) and kynurenine pathway in the regulation of the aging process. *Ageing Res Rev* 2022;75:101573.
PUBMED | CROSSREF

61. Norton DL, Ceppe A, Tune MK, McCravy M, Devlin T, Drummond MB, Carson SS, Vincent BG, Hagan RS, Dang H, et al. Bronchoalveolar Tregs are associated with duration of mechanical ventilation in acute respiratory distress syndrome. *J Transl Med* 2020;18:427.
PUBMED | CROSSREF

62. Xue Y, Xiao H, Guo S, Xu B, Liao Y, Wu Y, Zhang G. Indoleamine 2,3-dioxygenase expression regulates the survival and proliferation of *Fusobacterium nucleatum* in THP-1-derived macrophages. *Cell Death Dis* 2018;9:355.
PUBMED | CROSSREF

63. Blumenthal A, Nagalingam G, Huch JH, Walker L, Guillemin GJ, Smythe GA, Ehrt S, Britton WJ, Saunders BM. *M. tuberculosis* induces potent activation of IDO-1, but this is not essential for the immunological control of infection. *PLoS One* 2012;7:e37314.
PUBMED | CROSSREF